

The effects of geochemical reactions on CO₂ sequestration in deep saline aquifers

LE Nguyen Khoi^{1,2}, BUI Vinh Trong^{1,2}, MAI Lan Cao^{1,2,*}

¹ Faculty of Geology and Petroleum Engineering, Ho Chi Minh City University of Technology, 268 Ly Thuong Kiet Street, Dien Hong Ward, Ho Chi Minh City, Vietnam

² Vietnam National University Ho Chi Minh City, Dong Hoa Ward, Ho Chi Minh City, Vietnam

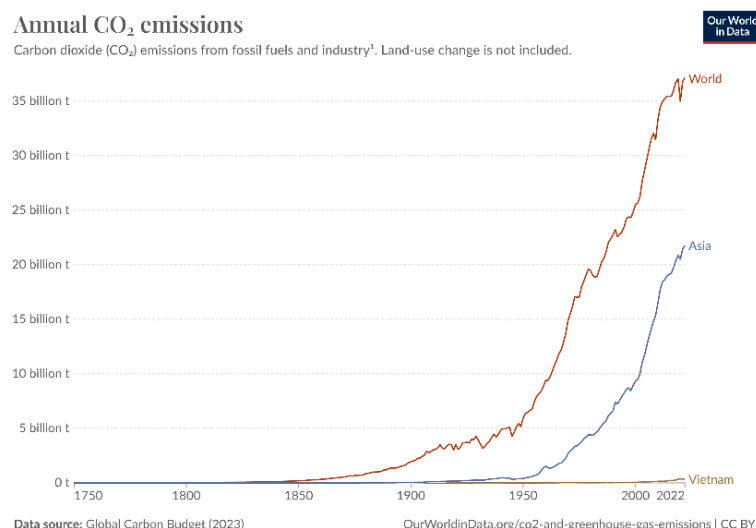
* Corresponding email: maicaolan@hcmut.edu.vn

Abstract: Deep saline aquifers are among the most promising geological formations for carbon sequestration due to their vast storage potential and long-term stability. However, CO₂ injection induces significant geochemical reactions that affect injectivity. This study investigates the impact of these reactions on reservoir properties during CO₂ injection, such as mineral dissolution/precipitation, pH variations, and changes in porosity and permeability. The simulation framework incorporates reaction stoichiometry modeling to quantify CO₂ interactions with formation water and minerals, validated using XRF and SEM-EDS data from Field X in Southern Vietnam. The results show that CO₂ injection caused some phenomena such as changes in mineral compositions and aqueous species distribution, particularly in the near-wellbore region. Minerals precipitation/dissolution release cation and HCO₃⁻, raising pH, while silicate dissolution contributes to acidification. These reactions lead to increased permeability and porosity, affecting CO₂ storage efficiency. Mineral precipitation/dissolution near the wellbore influences injectivity efficiency, emphasizing the need for accurate geochemical characterization.

Keywords: CO₂ injectivity; geological carbon sequestration; CO₂ geological storage; CO₂-brine-rock interactions

1. Introduction

The Industrial Revolution marked a significant era of technological advancement and economic growth, but it also led to severe environmental consequences, particularly through increased greenhouse gas emissions from fossil fuel consumption. The burning of coal, oil, and natural gas releases substantial amounts of carbon dioxide (CO₂) and other greenhouse gases, such as nitrous oxide and methane, contributing to the greenhouse effect. While this natural process is vital for regulating Earth's temperature, excessive greenhouse gas accumulation has intensified it, resulting in alarming global temperature increases [1]. According to recent statistical data published by Our World in Data, a project of the Global Change Data Lab, global CO₂ emissions in 2022 reached 37.15 billion tons, with 21.77 billion tons emitted in Asia [1], as shown in Fig. 1. This data highlights that annual CO₂ emissions are one of the key contributors to exacerbating global climate issues.



¹ Fossil emissions: Fossil emissions measure the quantity of carbon dioxide (CO₂) emitted from the burning of fossil fuels, and directly from industrial processes such as cement and steel production. Fossil CO₂ includes emissions from coal, oil, gas, flaring, cement, steel, and other industrial processes. Fossil emissions do not include land use change, deforestation, soils, or vegetation.

Fig. 1. Global CO₂ emissions from 1750 to 2022 [1]

Subsurface CO₂ storage is an effective solution for addressing environmental concerns and mitigating global warming, with depleted hydrocarbon reservoirs and deep saline aquifers being the most suitable sites due to their secure geological structures and high porosity and permeability. CO₂ storage in saline aquifers is particularly promising for long-term carbon sequestration. In these aquifers, carbonate minerals like calcite and dolomite are essential as they rapidly react with injected CO₂ dissolved in formation water, producing carbonic acid [2][3]. This leads to significant impacts on injection systems, causing the formation of new minerals through precipitation or the dissolution of original minerals in the reservoir rock. The dissolution/precipitation process of these minerals can alter the porosity and permeability of the formation, creating an urgent need to study the mechanisms of geochemical reactions in deep aquifers to ensure long-term storage and optimize the amount of CO₂ that can be injected into deep saline aquifers [3][4][5].

In addition to CO₂ dissolving in formation water, which readily reacts with carbonate minerals, there is still a lack of research on the impact of silicate minerals such as quartz, kaolinite, etc., on CO₂ sequestration. Most studies (numerical or experimental) have focused on investigating geochemical reactions in carbonate rocks, paying little attention to the short-term and long-term reactions between CO₂ dissolved in formation water and silicate minerals. This has led to difficulties in estimating the effects of silicates on the CO₂ injection and storage process. Therefore, the aim of this study is to identify the factors affecting CO₂ injectivity and the rock-fluid interactions between CO₂, formation water, and rock. The research will develop a model to predict the dissolution and precipitation of minerals in reservoir rocks containing both carbonates and silicates when reacting with CO₂ dissolved in formation water, while also examining changes in rock permeability and porosity during the CO₂ injection and storage process.

2. Methodology

The impact of geochemical reactions due to CO₂ injection into saline formations on the porosity and permeability of these formations is difficult to measure precisely, as there are many factors involved, such as changes in ion distribution, reaction rate, and the reaction time of the components in the aqueous and mineral environment of the reservoir. Furthermore, laboratory experiments are limited in terms of time and spatial scale. To address this, we used Computer Modelling Group – CMG software for simulation, allowing us to analyze these complex interactions more effectively.

2.1. General considerations

To calculate the dissolution/precipitation of minerals, changes in pH, CO₂-brine-rock interactions such as porosity and permeability, and to analyze CO₂ storage and the near-wellbore region during and after CO₂ injection. (Fig. 2). The sequential model construction process briefly as follows:

- First, data for the model was prepared, a static reservoir model with homogeneous by authors in this work. However, data inputs for simulation, including reservoir properties, fluid components, rock-fluid interactions, and initial conditions, were derived from core sample experiments (RCA and SCAL) from Field X (the actual field name is withheld per operator requirements) in Southern Vietnam, where porosity was measured by using the CMS-300TM by helium expansion and Klinkenberg permeability was assessed using the CMS-300TM UnsteadyState Permeameter, where helium flow and pressure decay were analyzed to calculate permeability. Moreover, initial mineral fractions and formation water species, X-ray Fluorescence (XRF) analysis is employed to quantify the elemental composition of rock samples, while Scanning Electron Microscopy (SEM), often coupled with Energy Dispersive X-ray Spectroscopy (EDS), provides detailed imaging and elemental analysis at the microscale [6].
- Next, during the injection of CO₂ into deep saline aquifers, the reaction stoichiometry is calculated immediately to determine how the injected CO₂ interacts with the existing ions and minerals in the subsurface. This initial step involves calculating the balance of chemical reactions between CO₂, formation water, and the surrounding minerals. By analyzing these interactions, we can determine the distribution of ions both in the aqueous phase (dissolved in the formation water) and within the mineral matrix (solid phase). The results obtained from this stoichiometric calculation are essential inputs for subsequent steps in the modeling process.
- Finally, the analysis results of mineral and aqueous components were used to interpret the impact of geochemical reactions on rock-fluid interactions, flow capacity, and the behavior of CO₂ near the wellbore region. Additionally, the model was utilized to evaluate CO₂ storage capacity in the reservoir over time.

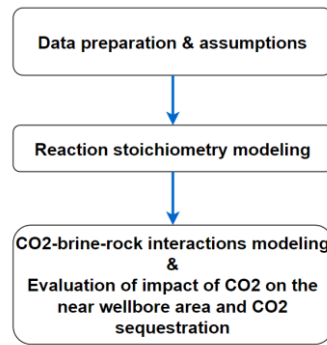


Fig. 2. Modeling process to assess the impact of CO₂ injection in deep saline aquifers

2.2. Reaction Stoichiometry Modeling

The steps involved in simulating the calculation of reaction stoichiometry are illustrated in detail in Fig. 3, which plays a crucial role in determining the distribution of ions in the aqueous environment. By accurately calculating the stoichiometry of the reactions, the model provides insight into which ions are released into or consumed by the aqueous environment. These species are key to understanding the chemical dynamics of the reservoir once CO₂ is injected. In addition to ion distribution, the model also calculates the dissolution and precipitation of minerals within the reservoir rock. The Saturation Index (SI) (see Section 2.2.2) is used to determine the tendency of specific minerals to dissolve or precipitate under the conditions created by CO₂ injection. Intra-aqueous reactions are homogeneous, involving only dissolved components and reaching equilibrium quickly, so they are modeled as chemical-equilibrium reactions. Mineral reactions, like dissolution or precipitation, are heterogeneous, involving minerals and aqueous species, and proceed slower, so they are represented as rate-dependent reactions. This distinction is vital for accurate geochemical modeling [7].

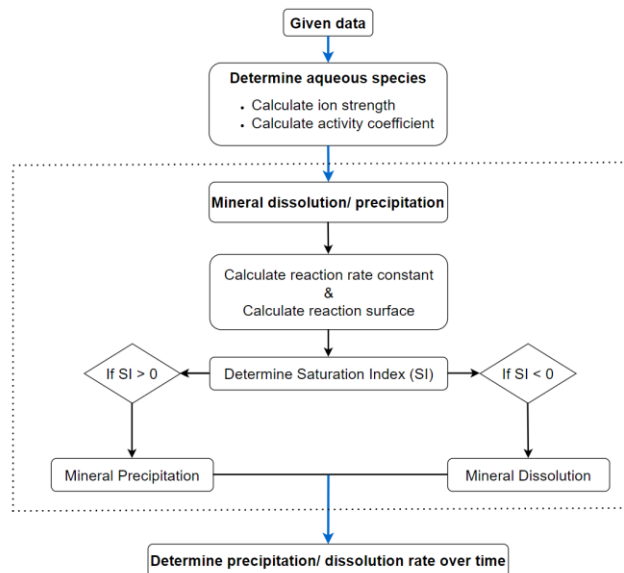


Fig. 3. Modeling process for stoichiometry reaction modeling

2.2.1. Determine aqueous species

Step 1: Calculate the ionic strength (I), the activity coefficient (γ) and activities (a_i)

The ionic strength of a mixture of several aqueous components is calculated based on two groups of coefficients, the charge of the ion and the molality (moles per kg of H₂O) proposed by Bethke [8] và Tanford [9] as follows:

$$I = \frac{1}{2} \sum_{i=1}^{n_{aq}} m_i z_i^2 \quad (1)$$

in eq. (1), n_{aq} is the number of components that exist only in the aqueous phase. z_i are the charge và the molality of the i^{th} ion, respectively.

For ideal solution, the activity coefficient is equal to the molality ($\gamma = 1$). However, for most cases, the solution is non-ideal and the preferred model for ionic activity coefficient is the B -dot model [8], and calculated as follows:

$$\log \gamma_i = -\frac{A_\gamma z_i^2 \sqrt{I}}{1 + \dot{a}_i B_\gamma \sqrt{I}} + \dot{B}I \quad (2)$$

$$a_i = \gamma_i m_i \quad (3)$$

in eq. (2), A_γ , B_γ and \dot{B} are temperature dependent parameters, \dot{a}_i is the ion size parameter, and I is the ionic strength.

Step 2: Determine aqueous species by performing the chemical equilibrium reactions

A reaction between species in the aqueous phase has the following stoichiometry:

$$\sum_{i=1}^{n_{aq}} v_{ij} A_i = 0, \quad j = 1, \dots, R_{aq} \quad (4)$$

in eq. (4), A_i is the chemical symbol for the i^{th} aqueous species, n_{aq} is the total number of components in the aqueous phase (including gaseous), and R_{aq} be the number of reactions between aqueous components.

Eq. (4) are modeled with chemical equilibrium constants [8]. The governing equations for the chemical equilibrium reactions are:

$$Q_j - K_{eq,j} = 0, \quad j = 1, \dots, R_{aq} \quad (5)$$

$$\prod_{i=1}^{n_{aq}} a_i^{v_{ij}} - K_{eq,j} = 0, \quad j = 1, \dots, R_{aq} \quad (6)$$

in eq. (5) and eq. (6), $K_{eq,j}$ is the chemical equilibrium constant for the aqueous reactions j and is provided as a table of values as function of temperature for any aqueous reactions [8][10], a_i is the activity of component i , v_{ij} are the stoichiometry coefficients and Q_j is the activity product.

2.2.2. Mineral dissolution/ precipitation is represented as rate-dependent reactions

As mentioned, reactions between aqueous-phase components happen rapidly compared to the slower processes of mineral dissolution and precipitation. Therefore, intra-aqueous reactions are considered chemical equilibrium reactions, while mineral dissolution and precipitation are described as rate-dependent processes.

Step 1: Calculate the reaction rate constant (k_j)

The reactions rate constants are normally reported in the literature at a reference temperature T_0 (usually 298.15 K or 25 °C) [11]. The following equation is used to calculate the rate constant at a different temperature T :

$$k_j = k_{0j} e^{-\frac{E_{aj}}{R} \left(\frac{1}{T} - \frac{1}{T_0} \right)} \quad (7)$$

in eq. (7), E_{aj} is the activation energy for reaction j (J/mol) – determined by measuring the reaction rate at various temperatures and applying the Arrhenius equation, which relates the rate constant to temperature [12] – and k_{0j} is the reaction rate constant for reaction j at T_0 (mol/(m²s)).

Step 2: Calculate the reactive surface area \hat{A}_j

The reactive surface area is another important parameter in the calculation of the reaction rate [13][14]. The following equation is used to calculate the reactive surface area with change in the moles of minerals through dissolution or precipitation:

$$\hat{A}_j = \hat{A}_j^0 \frac{N_j}{N_j^0} \quad (8)$$

in eq. (8), \hat{A}_j^0 is the reactive surface at time 0 – determined using gas adsorption techniques (BET method) [15], N_j is the mole number of mineral j per unit grid block volume at current time and N_j^0 is the mole number of mineral j per unit block bulk volume at time 0.

Step 3: Determine Saturation Index (SI)

The saturation index is also one of the important parameters contributing to the reaction rate. Based on the saturation index, we can determine which minerals in the reservoir rock undergo dissolution/precipitation. The following equation is used to calculate the saturation index:

$$SI = \frac{Q_j}{K_{eq,j}} = \frac{\prod_{i=1}^{n_{aq}} a_i^{v_{ij}}}{K_{eq,j}} \quad (9)$$

in the eq. (9), the product does not involve the activities of the minerals as they are equal to unity. The activity product Q_j is analogous to the activity product for aqueous chemical equilibrium reactions equation as eq. (6). The chemical equilibrium constants $K_{eq,j}$ for many minerals (both silicate and carbonates minerals) are also available in the literature [8][10].

When the Saturation Index (SI) is greater than 1 ($SI > 1$), it indicates that the solution is supersaturated with respect to a specific mineral, meaning that the concentration of dissolved ions exceeds the solubility limit of that mineral. As a result, mineral precipitation occurs. On the other hand, when the Saturation Index is less than 1 ($SI < 1$), it indicates that the solution is undersaturated with respect to the mineral, meaning that the concentration of dissolved ions is below the solubility limit. In this case, mineral dissolution occurs. When the Saturation Index equals zero ($SI = 0$), the system is in a state of equilibrium. At this point, the concentration of dissolved ions exactly matches the solubility of the mineral, and no net precipitation or dissolution occurs [16].

Step 4: Determine the rate of mineral dissolution/ precipitation (r_j)

The rate law for the mineral dissolution and precipitation reactions is [8]:

$$r_j = \hat{A}_j k_j \left(1 - \frac{Q_j}{K_{eq,j}} \right), \quad j = 1, \dots, R_{mn} \quad (10)$$

in eq. (10), r_j is the rate and R_{mn} is the number of reactions between minerals and aqueous components.

In this study, a specific convention is adopted to describe the reaction rates associated with mineral dissolution and precipitation processes in the reservoir. According to this convention, the reaction rate is considered negative when dissolution occurs ($SI < 1$). Conversely, the reaction rate is considered positive when precipitation occurs ($SI > 1$). When the ($SI = 1$), the reaction rate is zero, indicating that the system is in equilibrium. At this point, there is no net dissolution or precipitation of the mineral, meaning the concentrations of dissolved ions and the stability of the mineral are balanced.

2.3. Impact of CO₂ on rock-fluid interactions and underground CO₂ storage

The steps involved in the CO₂-brine-rock interaction model are illustrated in detail in Fig. 4, which plays an important role in determining the porosity and permeability in the reservoir and the pH in the aqueous environment during CO₂ injection.

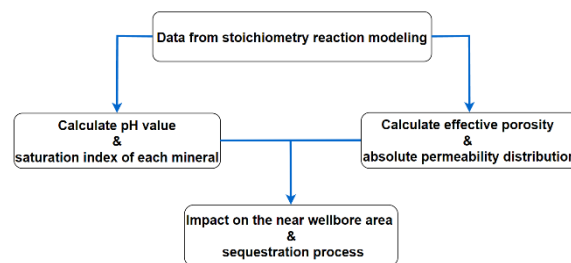


Fig. 4. Modeling procedure for CO₂-brine-rock interactions and CO₂ sequestration

2.3.1. Porosity calculation

Mineral dissolution increases porosity and permeability in porous media by creating new voids and expanding existing pores, while precipitation reduces pore size and can block flow paths. These alterations significantly impact fluid transport properties, influencing CO₂ storage, groundwater flow, and CO₂ migration in reservoirs. The porosity is calculated as follows [8]:

$$\hat{\phi}^* = \phi^* - \sum_{i=1}^{n_m} \left(\frac{N_j}{\rho_j} - \frac{N_j^0}{\rho_j} \right) \quad (11)$$

$$\phi = \hat{\phi}^* [1 + c_\phi (p - p^*)] \quad (12)$$

in eq. (11) and eq. (12), ϕ is the current porosity, ϕ^* is the reference porosity without mineral precipitation/ dissolution (initial porosity), $\hat{\phi}^*$ is the reference porosity including mineral precipitation/ dissolution, N_j is the mole number of mineral j per unit grid block volume at current time, N_j^0 is the mole number of mineral j per unit block bulk volume at time 0, ρ_j is the mineral molar density and c_ϕ is the rock compressibility, p^* is the reference pressure.

2.3.2. Permeability calculation

In eq. (11) and eq. (12), can be calculated the porosity of a porous medium by accounting for the changes in the mineral volume fraction, which directly impacts the pore structure. This approach allows us to evaluate how the dissolution or precipitation of minerals alters the void spaces within the medium. To further infer the permeability, we can apply the Kozeny-Carman formula, which provides a relationship between porosity, and permeability [17][18]:

$$\frac{k}{k^0} = \left(\frac{\phi}{\phi^0}\right)^3 \left(\frac{1 - \phi^0}{1 - \phi}\right)^2 \quad (13)$$

in eq. (13), k^0 and ϕ^0 are the initial permeability and porosity, respectively.

2.3.3. pH determination

During CO₂ injection into a reservoir, significant chemical reactions alter the pH, influenced by the dissolution or precipitation of minerals. In reservoirs containing carbonate minerals, the dissolution of minerals releases calcium ions (Ca²⁺) and bicarbonate ions (HCO₃⁻), leading to an increase in pH and creating a more alkaline environment [19]. In contrast, dissolving silicate minerals, such as feldspar or quartz, releases silica and other ions, often lowering pH and making the environment more acidic, resulting in complex geochemical interactions [20]. Accurately measuring the pH during CO₂ injection is crucial for understanding the reactions that impact reservoir properties like porosity and permeability. By calculating the changes in the moles of carbonate and silicate minerals, we can determine pH shifts over time.

2.3.4. Evaluation of the impact of CO₂ injection on the near-wellbore region and CO₂ sequestration

This section examines near-wellbore reactions and their influence on CO₂ sequestration capacity, focusing on ion distribution changes in aqueous and mineral environments alongside permeability and porosity alterations due to mineral dissolution or precipitation. The near-wellbore region is crucial for assessing the wellbore's integrity and reservoir storage capacity, as it experiences higher stresses during CO₂ injection. Factors such as pressure variations, injection flow rates, and the dissolution or precipitation of new minerals significantly impact CO₂ distribution and mineral reactivity. Numerical simulations serve as a primary tool for evaluating this process, offering insights into the complex interactions occurring during CO₂ injection. Furthermore, accurate characterization of numerical simulations has been shown to be effective in capturing hydrate formation, and salt precipitation, which are critical for understanding injectivity alterations and mechanical risks associated with CO₂ sequestration [21][22].

Changes in ionic composition in the near-wellbore area can lead to mechanical and chemical modifications in the rock formation. The precipitation of new minerals may create a mineral seal, reducing flow mobility in the reservoirs. The reservoir's ability to sequester CO₂ long-term after injection ceases relies on these reactions; new minerals can trap CO₂ as a solid phase, enhancing secure storage, while excessive dissolution may weaken the reservoir's structural integrity.

By analyzing these critical factors, this section aims to provide insights for optimizing the CO₂ injection process, ensuring effective and long-term sequestration of CO₂ in geological formations.

3. Results and Discussion

3.1. Input data and model assumptions

The input data for this study was obtained from field X in Southern Vietnam. The formation water was mixed from two formations, the Lower Miocene and the Upper Oligocene, with a total salinity of 43,000 ppm. The main lithology of the sample is light grey sandstone with siltstone lamination and veins. The sandstone primarily consists of quartz and plagioclase, with much smaller amounts of K-feldspars, and minor amounts of mica and rock fragments.

The main assumptions of the model in this study are:

- The injection well is a vertical well.
- The deep saline aquifer is homogeneous, with uniform permeability and porosity at every point.
- Isothermal conditions and pressure maintained throughout injection and sequestration time frame.

- The flow in the injection well is steady and unidirectional, from the top of the well to the bottom.

The descriptions of the wellbore, basic reservoir structural parameters, initial conditions and injection used in this simulation were shown in Tab. 1. Moreover, the initial mineral fractions and formation water species were determined by XRF and SEM analysis and presented in

Tab. 2. The main secondary minerals and the aqueous formula that might be occurred by geochemical reactions were shown in Tab. 3 [23].

Tab. 1. Reservoir parameters used in this study

Parameters	Values (sandstone formation from field X in Southern Vietnam)
Length (km)	15
Width (km)	15
Thickness (m)	50
Grid	50×50×10
Depth of top of reservoir (m)	1800
Porosity, ϕ	0.232
Horizontal permeability (mD), K_h	583
Vertical permeability (mD), K_v	$0.1 \times K_h$
Initial reservoir pressure (kPa)	18600
Initial reservoir temperature (°C)	50
Salinity of formation water (ppm)	43000
Water-gas contact (m)	1600
Injection rate (Million ton/year)	500
Perforation	Grid cells (25, 25, 8); (25, 25, 9); (25, 25, 10)
CO ₂ injection period (years)	16
CO ₂ sequestration period (years)	200

Tab. 2. Initial mineral component of the rock (left) and formation water species (right)

Sandstone Mineral compositions	Volume fraction (%)	Formation Water Species (ppm)	
Quartz	48.7	SO ₄ ²⁻	790
K-feldspar	42.6	Na ⁺	14637
Kaolinite	3.9	Cl ⁻	25250
Illite	1.8	K ⁺	136
Dolomite	2	Al ³⁺	0
Calcite	1	SiO ₂	121
		Mg ²⁺	281
		Ca ²⁺	1998
		HCO ₃ ⁻	0

Tab. 3. Possible dissolved/ precipitated mineral and aqueous phase in the modeling [23]

Mineral Reactions & Possible Secondary Minerals	Reactive surface area (m ² /m ³)	Activation Energy (J/mol)	Log10 reaction rate (1/sec)
Quartz = SiO ₂	7128	87500	-13.9
K-feldspar + 4(H ⁺) = (Al ³⁺) + 2H ₂ O + (K ⁺) + 3 SiO ₂	176	67830	-12
Calcite + H ⁺ = Ca ²⁺ + HCO ₃ ⁻	88	41870	-8.796
Dolomite + 2(H ⁺) = Ca ²⁺ + 2(HCO ₃ ⁻) + Mg ²⁺	88	41870	-9.222
Illite + 8(H ⁺) = 2.3(Al ³⁺) + 5H ₂ O + 0.6(K ⁺) + 0.25(Mg ²⁺) + 3.5 SiO ₂	26400	58620	-14
Kaolinite + 6(H ⁺) = 2(Al ³⁺) + 5H ₂ O + 2 SiO ₂	17600	62760	-8.796

Aqueous Reactions
$\text{CO}_2 (\text{aq}) + \text{H}_2\text{O} = \text{H}^+ + \text{HCO}_3^-$
$\text{H}^+ + \text{OH}^- = \text{H}_2\text{O}$
$\text{CO}_3^{2-} + \text{H}^+ = \text{HCO}_3^-$

3.2. Ion distribution in aqueous phase and mineralization in reservoir

Fig. 5, Fig. 6, Tab. 4, and Tab. 5 illustrate the geochemical composition changes within a deep saline aquifer after 16 years of continuous CO₂ injection, followed by a simulation extending 200 years into the future. These figures highlight the changes in the molar quantities of various ions in both the aqueous phase and mineral components. Upon injection, the CO₂ initially displaces existing fluids within the pore spaces of the reservoir. As CO₂ contacts the aqueous environment, it begins to dissolve at the gas-water interface, where it reacts with water to form carbonic acid (H₂CO₃). This acid rapidly dissociates into H⁺ ions and HCO₃⁻ ions [24], as summarized in Tab. 3.

Tab. 4. Change of dissolved (-) and precipitated (+) mineral compositions in 2025, 2125, and 2225

Mineral	Change of dissolved (-) and precipitated (+) mineral compositions (mole/m ³ pore volume) in 2025, 2125, and 2225		
	2025	2125	2225
Calcite	0.0000	-0.2442	-0.4920
Dolomite	0.0000	-0.0995	-0.2020
Kaolinite	0.0000	1.07x10 ⁻⁵	4.05 x10 ⁻⁵
K-feldspar	0.0000	2.66x10 ⁻¹⁰	3.58 x10 ⁻¹⁰
Quartz	0.0000	9.41x10 ⁻⁵	3.68x10 ⁻⁴
Illite	0.0000	-0.0017	-0.0035

Tab. 5. Solution species distribution and pH in 2025, 2125, and 2225

Solution species	Solution species distribution (mole/m ³ pore volume) and pH in 2025, 2125, and 2225		
	2025	2125	2225
Ca ²⁺	0.0000	0.3452	0.6963
Mg ²⁺	0.0000	0.1003	0.2034
HCO ₃ ⁻	0.0000	0.9043	1.8241
Al ³⁺	0.0000	0.0038	0.0079
H ⁺	0.0000	0.0008	0.0006
K ⁺	0.0000	0.0011	0.0023
SiO ₂	0.0000	0.0057	0.0118
pH	7.1004	4.9585	5.0316

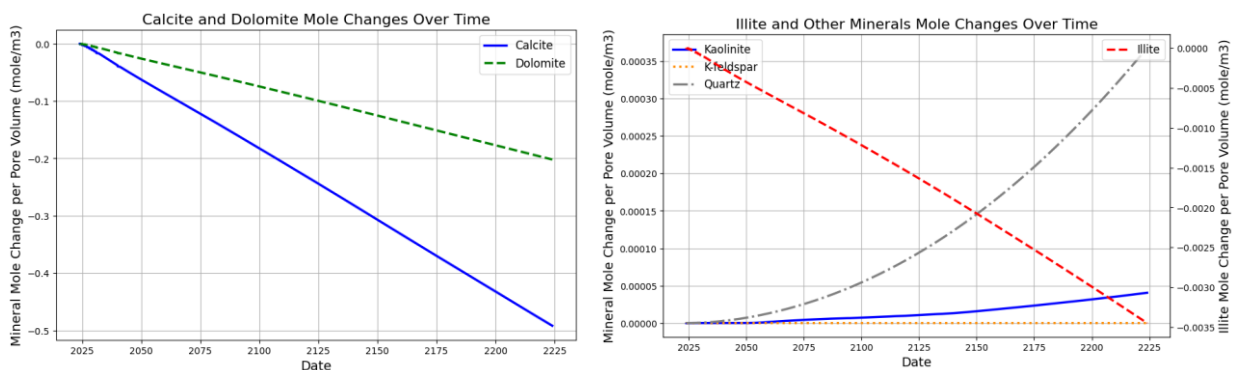


Fig. 5. Change of dissolved (-) and precipitated (+) mineral compositions over time (compared to the initial value at 2024)

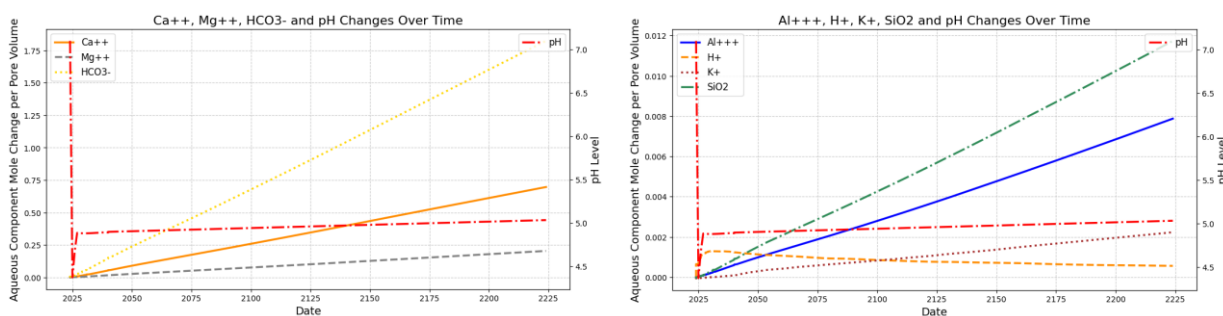


Fig. 6. Solution species distribution and pH over time (compared to the initial value at 2024)

The CO₂ injection process significantly increased H⁺ concentration, directly affecting the reservoir's pH levels. Initially, the pH dropped sharply from 7.0 to 4.4 as CO₂ dissolved, producing H⁺ ions. However, over time, due to the lower activation energy and faster reaction rate of carbonate minerals compared to silicate minerals, along with the rising presence of H⁺ ions, calcite and dolomite began to dissolve, acting as acid buffers that stabilized the pH around 5.1. This dissolution process also released Ca²⁺ and Mg²⁺ ions into the reservoir, with their presence steadily increasing throughout the 16 years injection and 200 years storage period. Moreover, the acidic environment also facilitates the partial dissolution of illite, a silicate mineral with a medium activation energy (lower than that of quartz, K-feldspar, and kaolinite). However, due to illite's very slow reaction rate, its dissolution over time is significantly less than that of carbonate minerals, with approximately 0.00345 mole/m³ pore volume dissolved after 200 years. This dissolution process releases ions such as K⁺, Mg²⁺, Al³⁺, and SiO₂ into the aqueous phase.

For other silicate minerals like kaolinite and K-feldspar to precipitate, a supply of aluminum is essential. This aluminum is sourced from the dissolution of aluminosilicates such as feldspar and illite. Additionally, sufficient concentrations of HCO₃⁻ and SiO₂(aq) are required for CO₂ to be effectively stored as calcite, kaolinite, or illite [25]. Simulation results show that quartz, kaolinite, and K-feldspar exhibit limited precipitation during the CO₂ injection phase following the Le Chatelier's principle, largely due to their high activation energy requirements and slower reaction rates, in contrast to other minerals in the system. However, during the storage phase, quartz begins to precipitate steadily, ultimately becoming the most significant precipitating mineral despite its high activation energy. By the end of the 200 years observation period, quartz precipitation reaches nearly 3.678x10⁻⁴ mole/m³ pore volume. Kaolinite and K-feldspar, while having lower activation energies and faster rates of precipitation than quartz, kaolinite's gradual precipitation reflects both its high activation energy and relatively faster reaction rate, leading to approximately 4.048x10⁻⁵ mole/m³ pore volume of precipitate by 200 years. In contrast, K-feldspar precipitates at a negligible rate throughout the study period due to its high activation energy combined with an exceptionally slow reaction rate, resulting in minimal accumulation of precipitate over time.

3.3. Evaluation of the impact of CO₂-fluid-rock interactions on the near wellbore

Fig. 7 and Fig. 8 illustrate the spatial distribution of CO₂ gas saturation, CO₂ aqueous mass fraction, and the dissolution/precipitation of certain minerals (calcite, dolomite, illite, quartz, and kaolinite) at various simulation times: 2 years, 16 years, 100 years, and 200 years. The injection well is located at the coordinate origin, assuming a homogeneous reservoir, with the survey area extending from the well out to a radius of 5100m.

CO₂ Gas Saturation and Aqueous Mass Fraction

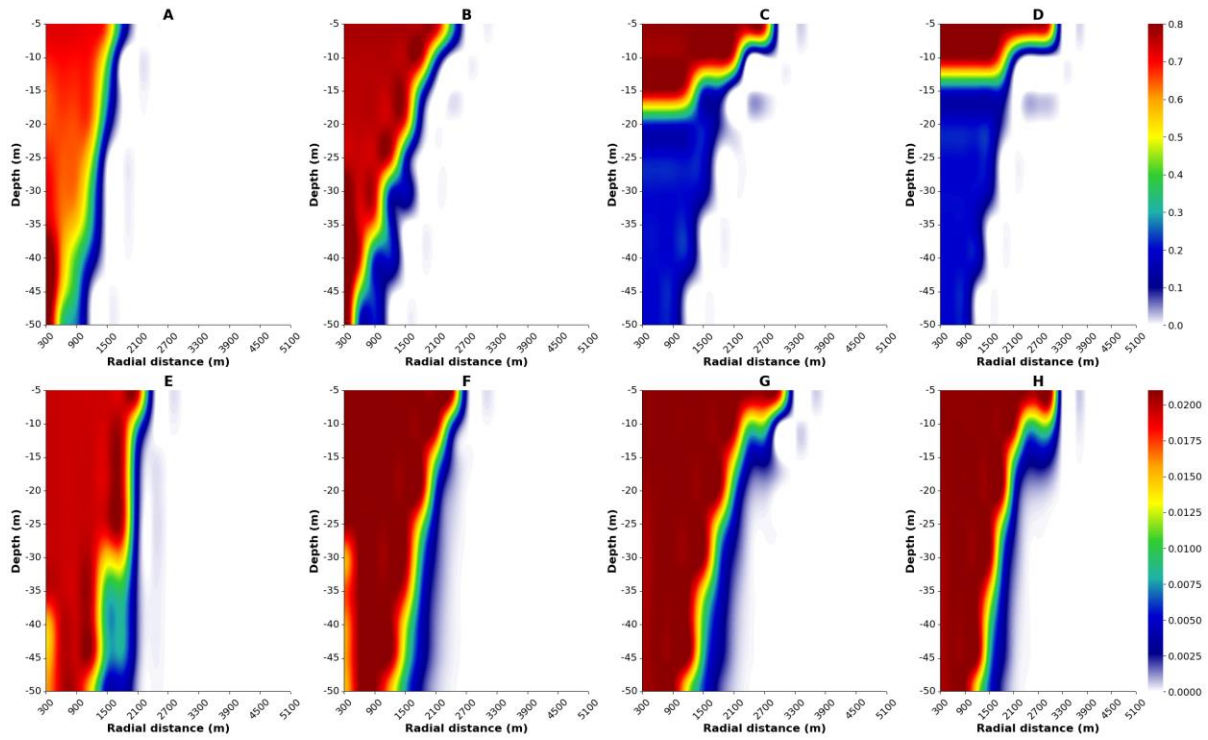
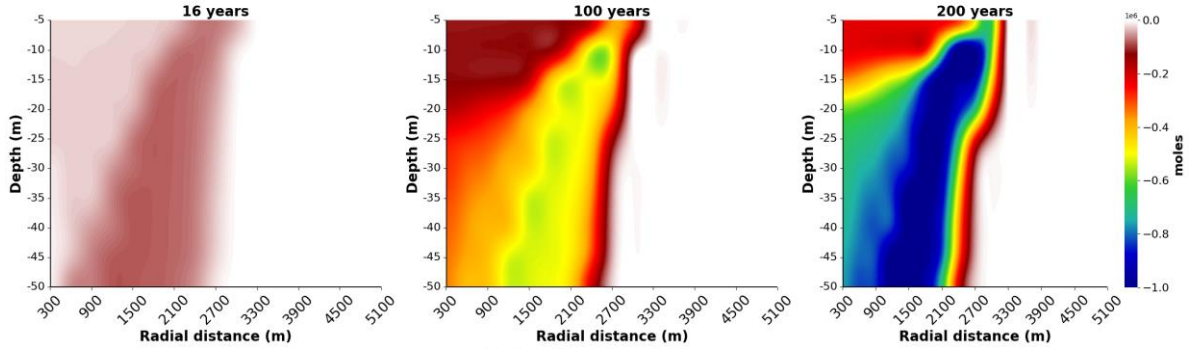
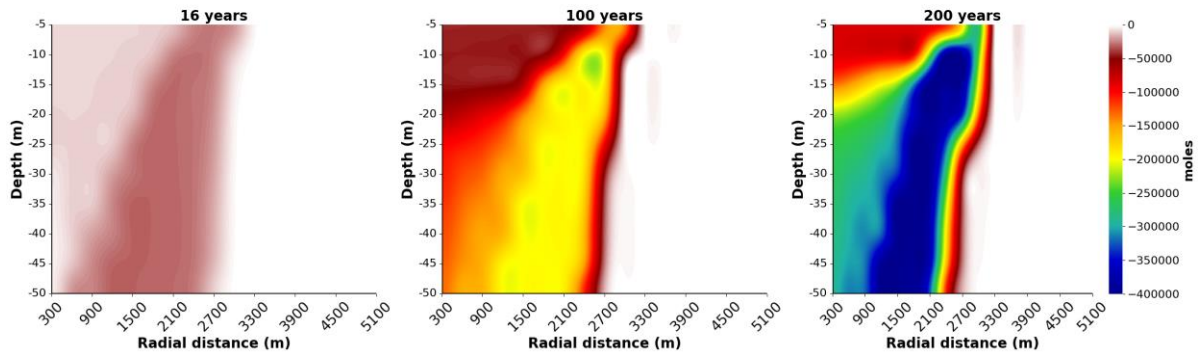


Fig. 7. Radial simulations of CO₂ injection into a homogeneous formation 50 m thick. Figures A, B, C, D at 2, 16, 100 and 200 years, show the gas saturation in the porous medium; and figures E, F, G, H at 2, 16, 100 and 200 years, show the mass fraction of dissolved CO₂ in the aqueous phase.

Calcite Dissolution



Dolomite Dissolution



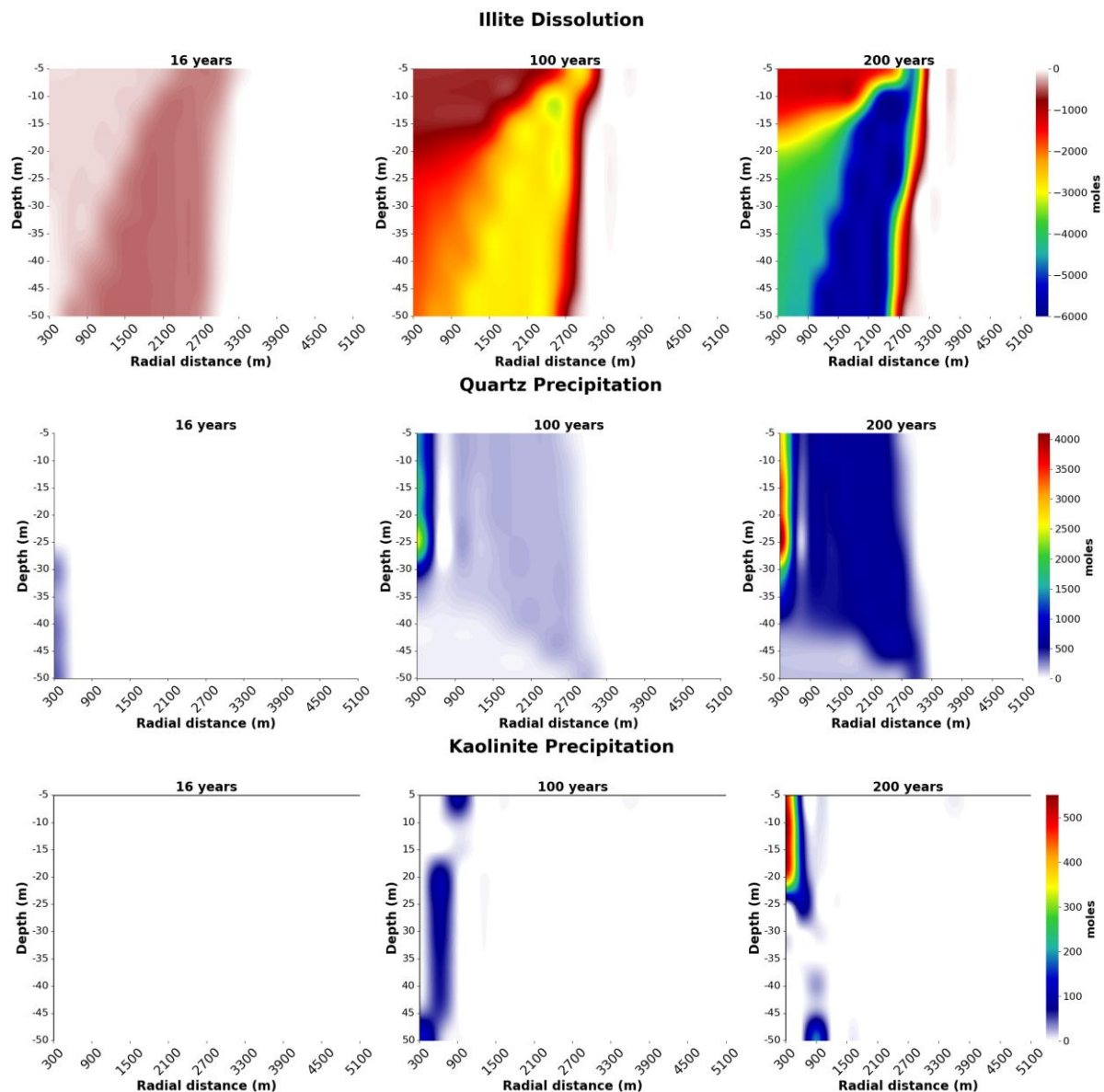


Fig. 8. The variations of mineral contents in the reservoir after 16, 100 and 200 years of compressed CO₂ energy storage (negative values indicate dissolution, positive precipitation).

Analyzing the simulation results reveals that CO₂ gas quickly migrates upward, accumulating in the uppermost layers beneath the cap rock. After CO₂ injection stops, the CO₂ gas continues to spread, reaching an influence radius of over 3200m after 200 years. Additionally, the front of CO₂ dissolved in brine moves downward from the top layer [26], also reaching an influence radius of more than 3200m after 200 years. Fig. 8 shows that injected CO₂ impacts the dissolution/ precipitation of minerals in the reservoir similarly to the trends observed in Figure 5. During the first two years of CO₂ injection, the dissolution of calcite, dolomite, and illite is negligible. After 16 years, dissolution levels remain low, but after 100 and 200 years of storage, the dissolution of calcite, dolomite, and illite increases, with calcite dissolving the most, followed by dolomite and illite. Conversely, quartz and kaolinite exhibit minimal precipitation during the initial CO₂ injection phase (16 years) and precipitate slowly and weakly near the well bottom after CO₂ storage. At distances beyond 3200m from the injection well, CO₂ gas saturation and CO₂ aqueous mass fraction are almost zero, and mineral dissolution and precipitation remain nearly nonexistent after 200 years. This indicates that the influence of CO₂ extends only to approximately 3200m, establishing an effective impact radius of about 3200m from the injection well.

Due to mineral dissolution, the reservoir’s porosity and permeability undergo slight changes, as shown in Fig. 9. Specifically, within a radius of approximately 3200m, porosity and permeability increase gradually and linearly over the 200-year period, with porosity rising from 0.232 to 0.2336 and permeability from 583 mD to 594 mD - an increase of around 0.05% from their initial values. This variation occurs because CO₂ migration and geochemical reactions are most active within this zone, where mineral

dissolution slightly enhances porosity and permeability. Beyond the 3200m radius, CO₂ concentration decreases significantly, leading to reduce geochemical interactions and stabilization of both permeability and porosity throughout the study. These findings suggest that mineral dissolution and precipitation under CO₂ influence have minimal impact on the reservoir's porosity and permeability, thus having a negligible effect on the long-term viability of CO₂ injection and storage.

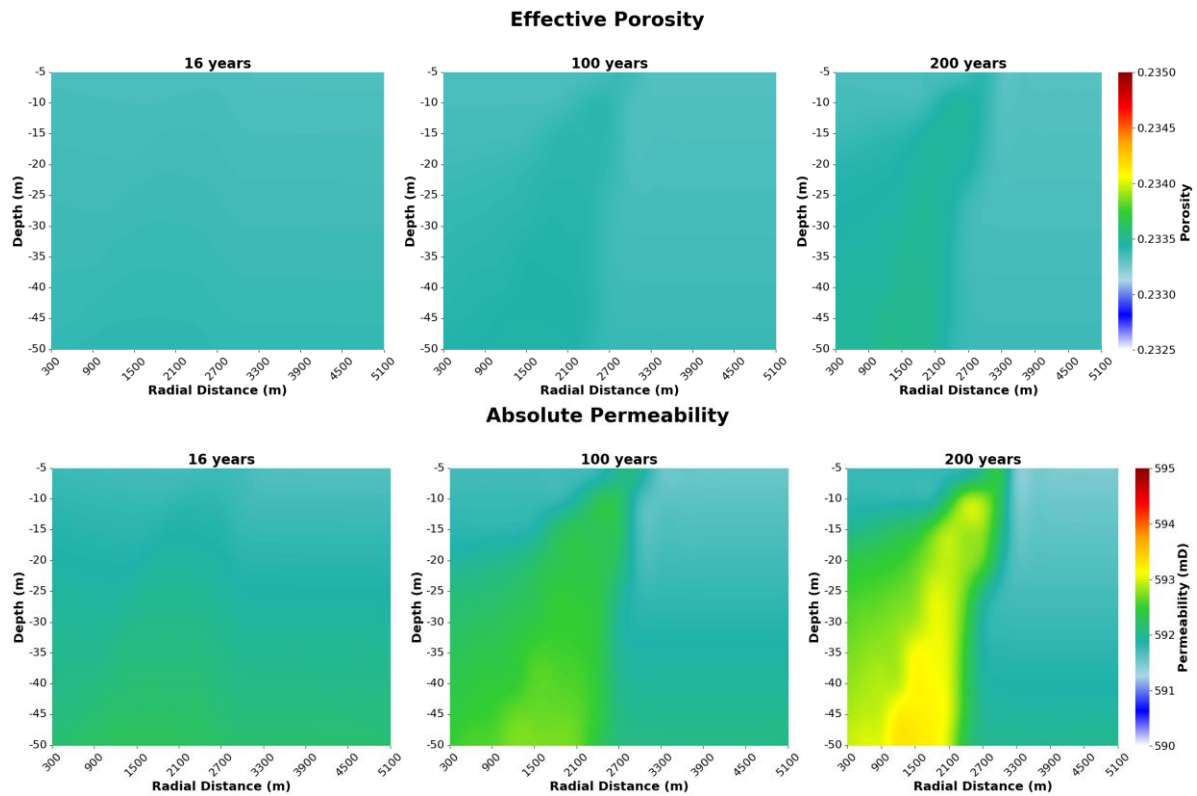


Fig. 9. The variations of effective porosity and absolute permeability in the reservoir after 16, 100 and 200 years of compressed CO₂ energy storage.

3.4. Evaluation of CO₂ sequestration capacity

During the storage of compressed CO₂ in deep saline aquifers, the injected CO₂ gradually dissolves into the formation water, interacting with various reservoir phases over time [27]. Fig. 10 illustrates the capture of CO₂ across different trapping mechanisms, including solubility trapping, structural trapping, mineral trapping, and CO₂ in aqueous phase.

When the CO₂ injection process begins, the amount of CO₂ in the formation increases rapidly trapped due to structural trapping, while the CO₂ dissolved in formation water also rises due to solubility trapping mechanism. This rapid increase continues throughout the injection phase and stabilizes in the subsequent period. By the end of the injection phase, the amount of CO₂ trapped reaches over 2.2×10^{11} mol and continues to increase slowly, reaching 2.6×10^{11} mol after 200 years. Dissolved CO₂ exceeds 5.6×10^{10} mol and continues to increase gradually, reaching 8×10^{10} mol after 200 years. This indicates that CO₂ continues to actively dissolve and is retained in the formation and aqueous phase even long after the injection process stops. CO₂ in the aqueous phase exhibits a similar trend but at a significantly lower retention level than the two other mechanisms. CO₂ in aqueous phase remains relatively stable at around 3×10^{10} mol over the entire study period. This continuous increase is due to dissolved CO₂ reacting with water formation and stabilizing as the geochemical system reaches equilibrium.

Due to the slow kinetics of geochemical reactions within the reservoir, CO₂ sequestration in the mineral phase progresses more gradually. After 16 years of CO₂ injection, the CO₂ trapped in mineral form amounts to only 1.88×10^8 moles, and this value slowly increases to 2.33×10^8 moles after 200 years, reflecting the time – intensive nature of mineralization processes such as precipitation. This relatively low absorption indicates that mineral trapping plays only a minor role in CO₂ sequestration compared to other mechanisms. The reason for this is not only the slow reaction kinetics but also the mineral composition of the reservoir. The studied reservoir is primarily composed of silicate minerals, while carbonate minerals such as calcite and dolomite, which have a much faster dissolution rate and react more readily with CO₂ are present in very low concentrations. This imbalance prevents the mineral trapping mechanism from reaching

its full potential, even though, theoretically, carbonate minerals could significantly accelerate CO₂ sequestration. This highlights the need for a more balanced ratio of silicate and carbonate minerals in the reservoir to optimize CO₂ injection and enhance the efficiency of CO₂ fixation in the mineral trapping.

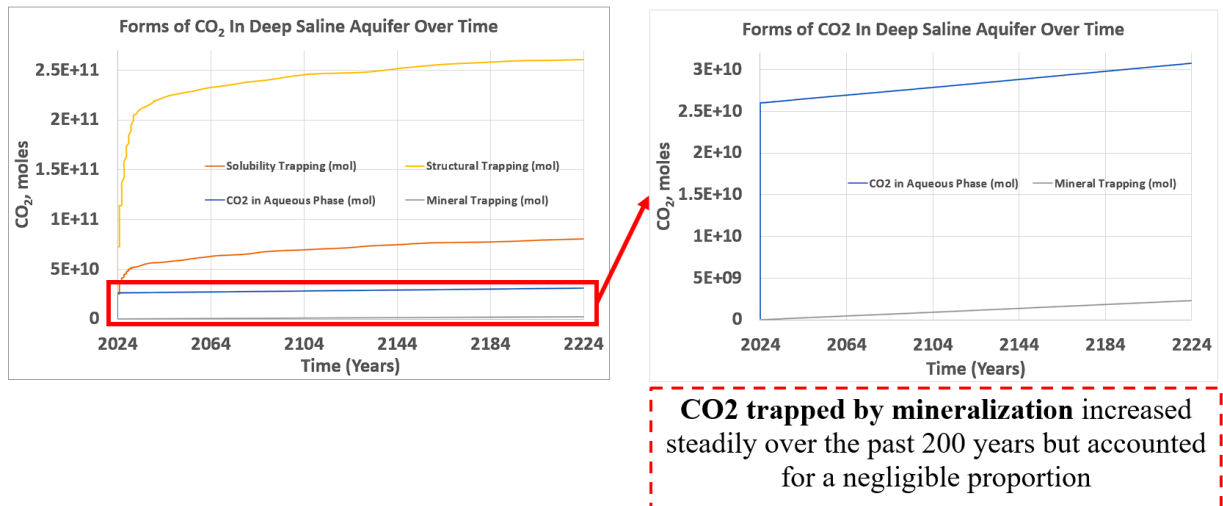


Fig. 10. CO₂ storage capacity at each trapping mechanism over 200 years

4. Conclusion

The results from numerical simulations of CO₂ sequestration in a sandstone formation reveal significant geochemical changes in the saline aquifer upon CO₂ injection. The initial injection lowers the pH due to carbonic acid formation, increasing H⁺ concentration. This acidic shift dissolves carbonate minerals like calcite and dolomite, buffering the environment and stabilizing the pH. Dissolution of these minerals’ releases Ca²⁺ and Mg²⁺ ions, which persist in the reservoir, indicating a dynamic adjustment in aqueous chemistry. Near the wellbore, minerals like calcite, dolomite, and illite dissolve quickly due to lower activation energies, while quartz, kaolinite, and K-feldspar precipitate at slower rates. The slight increase in porosity and permeability supports the reservoir’s long-term structural stability, confirming the feasibility of CO₂ injection and storage.

Finally, CO₂ sequestration in the aquifer occurs through a variety of trapping mechanisms, including structural, solubility and mineral trapping, each of which contributes to the interception of injected CO₂. Structural and dissolution trapping mechanisms dominate during the injection and subsequent stabilization periods, while mineral trapping occurs more slowly, with minor contributions over the 200-year observation period. The continued dissolution and retention of CO₂ in the aqueous phase emphasizes the potential of deep saline aquifers as long-term CO₂ storage sites, where slow geochemical processes ultimately enhance the stability and efficiency of sequestration over extended timescales.

Acknowledgements

This research is funded by Vietnam National University Ho Chi Minh City (VNU-HCM) under grant number DM2024-20-02. We acknowledge Ho Chi Minh University of Technology (HCMUT), VNU-HCM for supporting this study. We also greatly appreciate the support of Computer Modelling Group (CMG) in providing the software license for use in this research. Lastly, we thank the anonymous reviewers for their valuable feedback.

Literature - References

- [1] “Annual CO₂ emissions,” Our World in Data. Accessed: Mar. 28, 2025. [Online]. Available: <https://ourworldindata.org/grapher/annual-co2-emissions-per-country>
- [2] B. B. Hanshaw and W. Back, “Major geochemical processes in the evolution of carbonate—Aquifer systems,” *J. Hydrol.*, vol. 43, no. 1, pp. 287–312, Oct. 1979, doi: 10.1016/0022-1694(79)90177-X.
- [3] C. M. White, Strazisar ,Brian R., Granite ,Evan J., Hoffman ,James S., and H. W. and Pennline, “Separation and Capture of CO₂ from Large Stationary Sources and Sequestration in Geological Formations—Coalbeds and Deep Saline Aquifers,” *J. Air Waste Manag. Assoc.*, vol. 53, no. 6, pp. 645–715, Jun. 2003, doi: 10.1080/10473289.2003.10466206.

- [4] R. J. Rosenbauer, T. Koksalan, and J. L. Palandri, "Experimental investigation of CO₂-brine-rock interactions at elevated temperature and pressure: Implications for CO₂ sequestration in deep-saline aquifers," *Fuel Process. Technol.*, vol. 86, no. 14, pp. 1581–1597, Oct. 2005, doi: 10.1016/j.fuproc.2005.01.011.
- [5] T. A. Siqueira, R. S. Iglesias, and J. M. Ketzer, "Carbon dioxide injection in carbonate reservoirs – a review of CO₂-water-rock interaction studies," *Greenh. Gases Sci. Technol.*, vol. 7, no. 5, pp. 802–816, 2017, doi: 10.1002/ghg.1693.
- [6] M. Gräfe *et al.*, "Combined application of QEM-SEM and hard X-ray microscopy to determine mineralogical associations and chemical speciation of trace metals," *J. Environ. Qual.*, vol. 40, no. 3, pp. 767–783, 2011, doi: 10.2134/jeq2010.0214.
- [7] L. Nghiem, V. Shrivastava, and B. Kohse, "Modeling Aqueous Phase Behavior and Chemical Reactions in Compositional Simulation," Accessed: Mar. 28, 2025. [Online]. Available: <https://dx.doi.org/10.2118/141417-MS>
- [8] C. M. Bethke, *Geochemical and Biogeochemical Reaction Modeling*. Cambridge University Press, 2022.
- [9] C. Tanford, "Theory of Protein Titration Curves. II. Calculations for Simple Models at Low Ionic Strength," ACS Publications. Accessed: Mar. 28, 2025. [Online]. Available: <https://pubs.acs.org/doi/pdf/10.1021/ja01577a002>
- [10] J. M. Delany and S. R. Lundeen, "The LLNL thermochemical data base -- revised data and file format for the EQ3/6 package," Lawrence Livermore National Lab. (LLNL), Livermore, CA (United States), UCID-21658, Jul. 1991. Accessed: Mar. 28, 2025. [Online]. Available: <https://www.osti.gov/biblio/138193>
- [11] F. Dubnikova and A. Lifshitz, "Quantum Chemical and Rate Constant Calculations of Thermal Isomerizations, Decompositions, and Ring Expansions of Organic Ring Compounds, Its Significance to Combustion Kinetics," in *Rate Constant Calculation for Thermal Reactions*, John Wiley & Sons, Ltd, 2011, pp. 147–189. doi: 10.1002/9781118166123.ch6.
- [12] A. M. Bryan and P. G. Olafsson, "Activation energy determination: An organic chemistry experiment," *J. Chem. Educ.*, vol. 46, no. 4, p. 248, Apr. 1969, doi: 10.1021/ed046p248.
- [13] L. E. Beckingham *et al.*, "Evaluation of mineral reactive surface area estimates for prediction of reactivity of a multi-mineral sediment," *Geochim. Cosmochim. Acta*, vol. 188, pp. 310–329, Sep. 2016, doi: 10.1016/j.gca.2016.05.040.
- [14] F. Qin and L. E. Beckingham, "The impact of mineral reactive surface area variation on simulated mineral reactions and reaction rates," *Appl. Geochem.*, vol. 124, p. 104852, Jan. 2021, doi: 10.1016/j.apgeochem.2020.104852.
- [15] R. L. Sanders, N. M. Washton, and K. T. Mueller, "Measurement of the Reactive Surface Area of Clay Minerals Using Solid-State NMR Studies of a Probe Molecule," *J. Phys. Chem. C*, vol. 114, no. 12, pp. 5491–5498, Apr. 2010, doi: 10.1021/jp906132k.
- [16] T. E. Larson, A. M. Buswell, H. F. Ludwig, and W. F. Langelier, "Calcium Carbonate Saturation Index and Alkalinity Interpretations [with Discussion]," *J. Am. Water Works Assoc.*, vol. 34, no. 11, pp. 1667–1684, 1942.
- [17] F. D. E. Latief and U. Fauzi, "Kozeny–Carman and empirical formula for the permeability of computer rock models," *Int. J. Rock Mech. Min. Sci.*, vol. 50, pp. 117–123, Feb. 2012, doi: 10.1016/j.ijrmms.2011.12.005.
- [18] G. Li, X.-S. Li, and C. Li, "Measurement of Permeability and Verification of Kozeny-Carman Equation Using Statistic Method," *Energy Procedia*, vol. 142, pp. 4104–4109, Dec. 2017, doi: 10.1016/j.egypro.2017.12.332.
- [19] "Carbonate reservoirs and factors affecting calcium carbonate (limestone) dissolution. - Free Online Library." Accessed: Mar. 28, 2025. [Online]. Available:

<https://www.thefreelibrary.com/Carbonate%2Breservoirs%2Band%2Bfactors%2Bffecting%2Bcalcium%2Bcarbonate...-a0323659191>

[20] “Geochemical Impacts to Groundwater from Geologic Carbon Sequestration: Controls on pH and Inorganic Carbon Concentrations from Reaction Path and Kinetic Modeling | Environmental Science & Technology.” Accessed: Mar. 28, 2025. [Online]. Available: <https://pubs.acs.org/doi/abs/10.1021/es100559j>

[21] M. B. Wapperom, X. Lyu, and D. V. Voskov, “Accurate Modeling of Near-Wellbore Effects Induced by Supercritical CO₂ Injection: European Conference on the Mathematics of Geological Reservoirs,” *Eur. Conf. Math. Geol. Reserv.* 2022, 2022, doi: 10.3997/2214-4609.202244092.

[22] J. Huang *et al.*, “Fully Coupled Near-Wellbore Multiphase Poromechanics Simulation for CO₂ Storage,” Accessed: Mar. 28, 2025. [Online]. Available: <https://dx.doi.org/10.56952/ARMA-2023-0099>

[23] L. Nghiem, P. Sammon, J. Grabenstetter, and H. Ohkuma, “Modeling CO₂ Storage in Aquifers with a Fully-Coupled Geochemical EOS Compositional Simulator,” Accessed: Mar. 28, 2025. [Online]. Available: <https://dx.doi.org/10.2118/89474-MS>

[24] Y. Shi *et al.*, “Geochemical reaction of compressed CO₂ energy storage using saline aquifer,” *Alex. Eng. J.*, vol. 64, pp. 679–689, Feb. 2023, doi: 10.1016/j.aej.2022.11.031.

[25] P. Ranganathan, P. van Hemert, E. S. J. Rudolph, and P. Z. J. Zitha, “Numerical modeling of CO₂ mineralisation during storage in deep saline aquifers,” *Energy Procedia*, vol. 4, pp. 4538–4545, Jan. 2011, doi: 10.1016/j.egypro.2011.02.411.

[26] “Carbon Dioxide Capture and Storage — IPCC.” Accessed: Mar. 28, 2025. [Online]. Available: <https://www.ipcc.ch/report/carbon-dioxide-capture-and-storage/>

[27] T. Xu, J. A. Apps, and K. Pruess, “Numerical simulation of CO₂ disposal by mineral trapping in deep aquifers,” *Appl. Geochem.*, vol. 19, no. 6, pp. 917–936, Jun. 2004, doi: 10.1016/j.apgeochem.2003.11.003.